


Control of the coupling strength and linewidth of a cavity magnon-polariton

Isabella Boventer,^{1,2} Christine Dörflinger,² Tim Wolz,² Rair Macêdo ,³ Romain Lebrun,¹ Mathias Kläui,^{1,4,*} and Martin Weides^{2,3}

¹*Institute of Physics, Johannes Gutenberg University Mainz, 55128 Mainz, Germany*

²*Institute of Physics, Karlsruhe Institute of Technology, 76131 Karlsruhe, Germany*

³*James Watt School of Engineering, Electronics & Nanoscale Engineering Division, University of Glasgow, Glasgow G12 8QQ, United Kingdom*

⁴*Materials Science in Mainz, Johannes Gutenberg University Mainz, 55128 Mainz, Germany*



(Received 8 April 2019; accepted 15 November 2019; published 13 February 2020)

The full coherent control of hybridized systems such as strongly coupled cavity-magnon states is a crucial step to enable future information processing technologies. Thus, it is particularly interesting to engineer deliberate control mechanisms such as the full control of the coupling strength which can act as a measure for coherent information exchange. In this work, we employ cavity resonator spectroscopy to demonstrate the complete control of the coupling strength of hybridized cavity-magnon states. For this, we use two driving microwave inputs which can be tuned at will. For these inputs, both the relative phase ϕ and relative amplitude ratio δ_0 can be independently controlled. We demonstrate that for specific quadratures between both tones we can increase the coupling strength, close the anticrossing gap, and enter a regime of level merging. At the transition, the absolute cavity signal is modified by 30 dB and we observe an additional linewidth decrease of 13% at resonance level merging. This kind of control over the coupling, and hence linewidth, opens an avenue to enable or suppress an exchange of information and bridges the gap between quantum information and spintronics applications.

DOI: [10.1103/PhysRevResearch.2.013154](https://doi.org/10.1103/PhysRevResearch.2.013154)

I. INTRODUCTION

Polaritons are the quasiparticles associated with the coupling of electromagnetic waves with an excited state of matter [1,2]. Such hybridized systems are promising candidates for applications as they can combine the advantages of the different physical systems and overcome the limitations of a single one [3–5]. While hybrid quantum circuits represent a tool for the deliberate control of quantum states, polaritons originating from light-matter interactions can be considered as a tool to study macroscopic systems through different kinds of hybrid systems such as exciton-photon or magnon-polaritons (MPs) [6–13]. For instance, MPs enable examining the spin-photon interaction, where the magnons are the associated quanta of a collective spin excitation [14]. The study and manipulation of spin-photon interactions could lead to the development of spintronic applications [15–20]. However, realizing such applications requires full control over the macroscopic coupling strength $g_{\text{eff}} = g_0\sqrt{(2NS)}$, where g_0 is the single spin coupling strength, N is the total number of contributing spins and S the spin number of the utilized material [21,22]. Since it represents a measure for the coherent information exchange, achieving full control over g_{eff} would enable the

deliberate enhancement or suppression of the information exchange [23]. This is of broad interest and has been studied for various systems such as single atoms, optomechanical circuits, exciton or surface plasmon-polaritons, and nanocavity-quantum dot systems [24–28].

Within cavity magnon-polariton (CMP) spectroscopy, various recent experiments studied MPs using an yttrium-iron-garnet (YIG) sphere as the magnonic sample in a cavity resonator with a *single* microwave signal as an input. At resonance, the photon states fully hybridize with the magnon states, creating a CMP [29] as originally predicted in Ref. [21]. In the strong coupling regime, g_{eff} is related to the anticrossing gap by $\Delta\omega = 2g_{\text{eff}}$ and set by the resonator geometry and the sample [22,30]. CMPs have been well studied for different configurations in recent years [16,20,29,31–39]. At room temperature, the origin of the coherent cavity-magnon coupling can be attributed to a fixed phase correlation of the electromagnetic fields [29]. By finding a possibility to tune the phase relation between the cavity photon and the magnon, g_{eff} could be manipulated. This has been recently shown to be possible when changing the position of the sample inside the cavity [40] and theoretically predicted in the case when a second field is introduced driving only magnons [41]. Here, we report on a tunable, and in principle also on-chip compatible, approach which allows full external control over the coupling strength g_{eff} , and thus of the hybridized states.

Specifically, the coupling strength is tuned by controlling the relative phase ϕ and amplitude ratio δ_0 between the cavity field and the corresponding field of a newly introduced second microwave drive. This second drive acts only on the magnons and it is not coupled to the cavity field generated from the

*klaui@uni-mainz.de

Published by the American Physical Society under the terms of the [Creative Commons Attribution 4.0 International](https://creativecommons.org/licenses/by/4.0/) license. Further distribution of this work must maintain attribution to the author(s) and the published article's title, journal citation, and DOI.

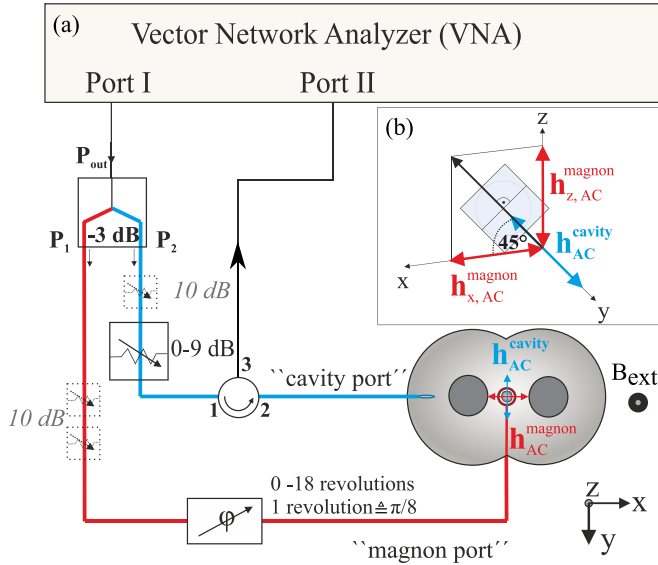


FIG. 1. (a) Schematics of the experimental setup showing the coherent signal from port I [output power level -5 dBm (0.3 mW)] divided by a power splitter. The value for δ_0 is controlled by a variable (0 to 9 dB) permanently inserted attenuator in the path of the cavity port and, if necessary, fixed attenuators (10 dB each). A mechanically tunable phase shifter in the path of the magnon port modulates the phase (uncertainty of $\pm 0.02\pi/8$). The system's response is measured in reflection at port II. (b) Orientation of the coupling loop and alignment of the intracavity magnetic fields (cf. Ref. [49]).

cavity port, which corresponds to the only microwave drive employed in previous experiments on single-input driven CMPs (e.g., in Refs. [22,30,40]).

Then, by simply controlling these inputs, the anticrossing gap can be enhanced or closed, leading to “level merging” exactly at the transition and level attraction beyond the closure of the gap. As we focus here on the special transition point of “level merging,” we discuss the impact of changing ϕ and δ_0 on the linewidth and total amplitude (in power units), which is beyond simple interference of the cavity photon and magnon response. In contrast to other works, our approach is entirely externally tunable. It is not necessary to modify the experimental environment such as moving the magnonic sample in the cavity resonator or changing the resonator geometry [40,42,43].

II. REALIZING AND MODELING A TWO DRIVE EXPERIMENT

Our experiment consists of a commercially bought YIG sphere ($\text{Y}_3\text{Fe}_5\text{O}_{12}$, $r = 0.1$ mm) [44], placed in the antinode of the alternating current (AC) magnetic field of a reentrant cavity resonator with $\omega_c/2\pi = 6.50$ GHz [45–48]. The additional input, called magnon port, is composed of a metallic loop around the YIG sphere (cf. Ref. [49]). Its driving field acts only on the magnons and does not couple directly to the cavity photons [cf. Fig. 1(b)]. Experimentally, we observe a direct coupling of the signal from the magnon port to the cavity photons. This coupling is what we denote as crosstalk

and it is measured as a transmission signal at the cavity port; i.e., it overlaps with the reflection measurement of interest (cf. Ref. [49]). However, the contribution of crosstalk can be neglected for the low- δ_0 regime ($0 < \delta_0 \cong 1$) discussed in this work, as it has no impact on the signal from the reflection measurement. The vector network analyzer (VNA) serves as the only microwave source to obtain two coherent microwave drives up to this phase and we measure in reflection [$S_{11}(\omega)$] [cf. Fig. 1(a)]. While ϕ is modulated by a mechanically tunable phase shifter added to path P_1 , the relative amplitude of both tones is controlled by the attenuators inserted in both paths.

The time-varying intracavity magnetic fields drive the spins in the YIG sphere out of equilibrium. Their dynamics can be described by the Landau-Lifshitz-Gilbert equation [50]. Here, we can quote the effective field acting on the magnetization dynamics as $\mathbf{H}_{\text{eff}} = \mathbf{H}_{\text{ext}} + \mathbf{h}_{\text{AC}}^{\text{cavity}} + \mathbf{h}_{\text{AC}}^{\text{magnon}}$, where $\mathbf{H}_{\text{ext}} = (0, 0, H_{\text{ext}})$ describes the external static magnetic field, $\mathbf{h}_{\text{AC}}^{\text{cavity}}$ denotes the AC field from the cavity port, and $\mathbf{h}_{\text{AC}}^{\text{magnon}} = \delta_0 e^{i\phi} \mathbf{h}_{\text{AC}}^{\text{cavity}}$ is the magnon port, driving magnons only. Thus, the relative phase and amplitude ratio are defined as $\phi = |\phi_{\text{cavity}} - \phi_{\text{magnon}}|$ and $\delta_0 = \frac{|\mathbf{h}_{\text{AC}}^{\text{magnon}}|}{|\mathbf{h}_{\text{AC}}^{\text{cavity}}|}$. Experimentally, we control the external amplitude ratio δ_{ext} and derive the internal ratio δ_0 by fitting Eq. (2) to our data (cf. Ref. [49]).

We focus on controlling the Kittel mode's coupling strength with wave vector $\mathbf{k} = 0$ and a linear dispersion $\omega_m = \gamma H_{\text{ext}}$ [51,52].

Our direct external drive on the magnons by the magnon port establishes an open system and is described by $\mathcal{H}_{\text{tot}} = \mathcal{H}_{\text{bath}} + \mathcal{H}_{\text{sys}}$, where $\mathcal{H}_{\text{bath}}$ denotes the microwave feed-line couplings including the microwave drives at either port and \mathcal{H}_{sys} is the interactions in the cavity including the coupling strength. For the description of the coupling strength of our two-tone driven CMP, we neglect $\mathcal{H}_{\text{bath}}$ (cf. Ref. [49]). In order to model our open system, we introduce the non-Hermitian Hamiltonian $\mathcal{H}_{\text{sys}} = \hbar\omega_c a^\dagger a + \hbar\omega_m m^\dagger m + \hbar g_{\text{eff}}(m^\dagger a + a^\dagger m) + \hbar\Omega(a^\dagger m)$. The penultimate term denotes the intracavity cavity photon-magnon interaction. The magnon port's contribution as an indirect drive to the cavity photons via the coupling of the magnons is considered in the last term by the “driving frequency” $\Omega = g_{\text{eff}}\delta_0 e^{i\phi}$.

The reflection scattering parameter $S_{11}(\omega)$ can be derived employing input-output theory (including the bath contributions) as [23]

$$S_{11}(\omega) = -1 + \frac{2\kappa_{e,1} - \frac{2ig_{\text{eff}}\delta_0 e^{i\phi}(1+\delta_0 e^{i\phi})\sqrt{\kappa_{e,1}\kappa_{e,2}}}{-i(\omega-\omega_m)+\kappa_m}}{-i(\omega-\omega_c) + \kappa_r + \frac{g_{\text{eff}}^2(1+\delta_0 e^{i\phi})}{-i(\omega-\omega_m)+\kappa_m}}, \quad (1)$$

where $\kappa_{e,1}$, $\kappa_{e,2}$, κ_r , and κ_m denote the dissipation parameters due to the coupling of the feedline into the resonator at the magnon and cavity port, the total resonator losses, and the magnon linewidth, respectively.

III. RESULTS AND DISCUSSION

Our findings begin by comparing the expressions for a one-port driven CMP [47] with Eq. (1), we introduce a new expression of the coupling strength considering the

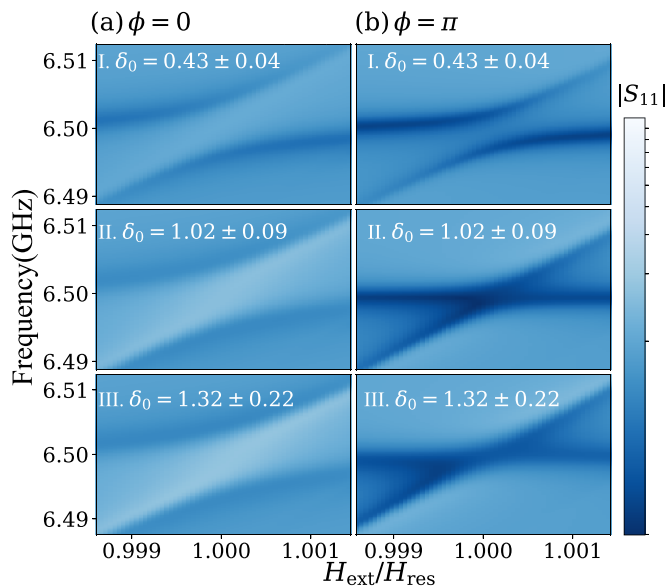


FIG. 2. Experimental spectra for (a) $\phi = 0$ and (b) $\phi = \pi$ for three different regimes of δ_0 : In I we see level repulsion [$\delta_0 < 1$], in II the transition [$\delta_0 \simeq 1$], and in III level merging [$\delta_0 > 1$]. The different combinations of values for ϕ and δ_0 lead to different effective couplings, i.e., $g'(\delta_0, \phi)$. Note that level repulsion is always observed for $\phi = 0$. All plots are normalized by the mean value of the signal's background amplitude and displayed in units of the resonance field H_{res} , i.e., where $\omega_c = \omega_m$.

dependence on ϕ and δ_0 as

$$g'(\delta_0, \phi) = g_{\text{eff}} \sqrt{1 + \delta_0 e^{i\phi}}, \quad (2)$$

where the value of g_{eff} denotes a complete suppression of the magnon drive ($\delta_0 = 0$) and for certain combinations of δ_0 and ϕ , Eq. (2) becomes complex and leads to level attraction (cf. Figs. 2(b) II, 2(b) III, and 3). This observation is also in line with the sign change for level merging shown in Ref. [25]. In addition, the analytical expectation from Eq. (2) is in accordance with the experimental data and the theoretical expectation of Ref. [41] for Fig. 3(c). As can be inferred from Eq. (2), the modulus of the coupling strength contains a nonzero imaginary part. If $|\text{Im}(g')| > |\text{Re}(g')|$, that is, the imaginary contribution dominates, the interaction potential between the cavity photons and the magnons changes from repulsive to attractive and the transition to the regime of level attraction is observed. To date, the occurrence of level attraction in a strongly coupled cavity photon-magnon system is associated to the dominance of a dissipative instead of a coherent coupling [25,41,53,54] regime. Hence, by our external control of the imaginary part, associated to controlling the amount of dissipative coupling in the expression for the coupling strength, we can obtain level attraction with our two-input driven approach. However, in our approach, the magnon is directly addressed by the fields from the second microwave input port. This approach is in stark contrast to single-input driven systems (e.g., Ref. [40]), where, instead, the dissipative coupling regime is reached by a modulation of the cavity resonator photon [53,54]. Another ansatz to explain the sign change in the interaction potential and, hence, occurrence

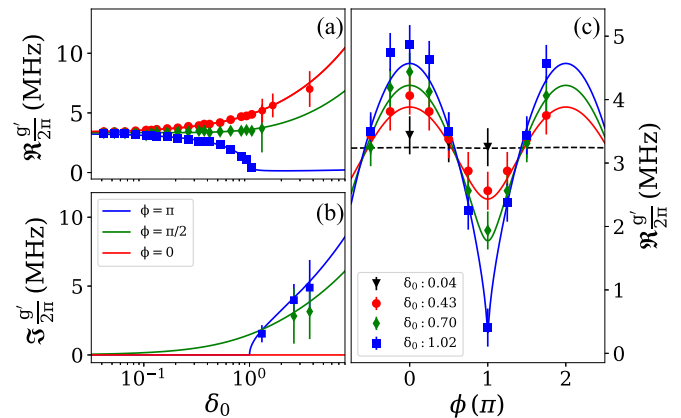


FIG. 3. Dependence of the real (a) and imaginary (b) parts of the coupling strength on δ_0 for $\phi \in \{0, \pi/2, \pi\}$. For all ϕ , the real part value merges to the same value within the error bars at very low δ_0 . For $\phi = 0$ (red circles) and $\phi = \pi/2$ (green diamonds), the coupling strength increases. However, higher values of the coupling strength are seen for $\phi = 0$. For $\phi = \pi$ (blue squares), we see a decrease toward the limit $\delta_0 \rightarrow 1$ where $g'(\delta_0, \phi)$ disappears. These behaviors are related to the imaginary part shown in panel (b). While for $\phi = \pi/2$ this increase is suppressed as real (level repulsion) and imaginary (level attraction) parts are nonzero, for $\phi = \pi$ only $\text{Im}(g'(\delta_0, \phi))$ is nonzero. (c) Experimental data (points) and fit (solid lines) of $\text{Re}(g'(\delta_0, \phi))|_{\delta_0=\text{const}}$ for four different values of δ_0 , confirming the findings in panel (a). The value to δ_0 is calculated from the fit result of panels (a) and (b) (cf. Ref. [49]). The solid lines are fits of Eq. (2).

of level attraction in CMP systems is the introduction of a diamagnetic response [55] induced by changing the sample position within the cavity's AC magnetic field. However, this effect is not present in our system. We do not alter the system and modulate the interaction potential by the effective magnetic fields acting on the magnons.

In the following, we first summarize the key features of our work by showing the spectra for relative phase shifts of Fig. 2(a) for $\phi = 0$ and Fig. 2(b) for $\phi = \pi$ for three different regimes of δ_0 . These are below ($\delta_0 = 0.43 \pm 0.04$, part I), at the transition ($\delta_0 = 1.02 \pm 0.09$, part II), and in the regime of level merging ($\delta_0 = 1.32 \pm 0.22$, part III). Then, we are going to examine the dependence of the coupling strength on δ_0 and ϕ in more detail (cf. Fig. 3), before we focus on the special case of level merging ($\phi = \pi$, $\delta_0 = 1$, cf. Fig. 4 in Ref. [49]). As expected from Eq. (2), for $\phi = 0$, the anticrossing gap increases towards higher δ_0 . In the regime of level merging for $\phi = \pi$, the imaginary part of the coupling term dominates the changes, resulting in level attraction [cf. Fig. 2(b), part III].

The dispersion spectrum of the CMP changes for various combinations of δ_0 and ϕ because the AC magnetic field from the magnon port exerts an additional torque on the precessing magnetization where its orientation depends on ϕ [41]. Furthermore, the transmission coefficient's amplitude and linewidth depend on the interplay (controlled by δ_0 and ϕ) between individual dissipation and coupling strength between the cavity photon and the magnon. For the specific case of level merging ($\phi = \pi$, $\delta_0 = 1$) and on resonance, this additional torque compensates the intrinsic damping and coupling-induced linewidth broadening. Being a measure for the energy

exchange between cavity photons and magnons, the coupling quantified by the coupling strength can be considered as an additional channel for energy dissipation for one subsystem or gain for the other subsystem within a single oscillation period for the energy exchange. Thus, for a dominating imaginary part in Eq. (2), the dissipative coupling is the strongest contribution which results in level attraction. Depending on the orientation of the effective acting torque (with contributions by both tones), the damping of the magnons is either enhanced or compensated for $\delta_0 = 1.02 \pm 0.09$ [cf. Fig. 2(b), part II]. Hence, a strong absolute change $|\Delta A|^2$ of the signal of $S_{11}(\omega)$ and decrease of the linewidth at level merging are expected at resonance.

Figure 3 shows the dependence of real [Fig. 3(a)] and imaginary [Fig. 3(b)] parts of $g'(\delta_0, \phi)$ for $\delta_0 = \text{const}$ and $\phi \in \{0, \pi/2, \pi\}$ and the real part for $\phi = \text{const}$ [Fig. 3(c)], including a fit based on Eq. (2) for the same range of δ_0 and ϕ . While $\text{Re}[g'(\delta_0, \phi)]$ was determined from the minimal gap distance evaluating both the amplitude and phase data (cf. Ref. [49]), the imaginary contribution for $\phi \neq 0$ and $\delta_0 > 1$ was extracted from the horizontal width of level merging, which corresponds to $4\text{Im}[g'(\delta_0, \phi)]$ [cf. Figs. 3(a) and 3(b)] [25,49]. For $\delta_0 \rightarrow 0$, the three curves merge and $g'(\delta_0, \phi) = g_{\text{eff}}$ as the influence of ϕ on $g'(\delta_0, \phi)$ vanishes. The cavity driven photon-magnon coupling dominates and results in an anticrossing gap of $2g'(\delta_0 \rightarrow 0)$. Since for $\phi = 0$, $\text{Im}[g'(\delta_0, \phi)] = 0$ for all δ_0 , and $\text{Re}[g'(\delta_0, \phi)] = 0$ for $\phi = \pi$ and $\delta_0 \geq 1$, the real part can be attributed to a repulsive interaction (anticrossing) and the imaginary part to an attractive one (level merging). In accordance with the expectation from Eq. (2) [cf. Fig. 3(a)] for $\phi = 0$, $\text{Re}[g'(\delta_0, \phi)] = 0$ increases toward $\delta_0 = 1$. On the other hand, for $\phi = \pi$ and $\delta_0 < 1$, the increasing contribution from the additional torque decreases the gap. The increase is lower than the total decrease at $\phi = \pi$, because here the coupling strength is “just” increased by $g'(\delta_0, 0) \propto \sqrt{1 + \delta_0}$. Furthermore, for $\phi = \frac{\pi}{2}$, we also observe a coexistence of anticrossing and level merging (cf. Ref. [58]). This results in a smaller increase for $\text{Re}[g'(\delta_0, \phi = \pi/2)]$ and demonstrates the broad tunability of our system. Figure 3(c) confirms both that the two-tone driven CMP can be effectively described as a single-tone driven CMP with $g' \equiv g_{\text{eff}}$ for $\delta_0 \rightarrow 0$ (black triangles), and that the onset of level merging is observed for $\phi = \pi$ and $\delta_0 = 1$ [cf. Fig. 3(c), blue squares].

Previously, for a CMP created by the cavity port only, an increase of the signal’s linewidth at resonance has also been reported [40]. However, in the transition to level merging, a decrease in linewidth accompanied by a strong absolute change of the resonance amplitude is expected [41]. As shown in Fig. 4, we observe an absolute change of the signal in power units by 30 dB and decrease in linewidth at the level merging transition for $\delta_0 = 1$ and $\phi = \pi$ below the simple addition of the cavity photon’s and the magnon’s linewidth from interference. Figure 4(a) shows the relative increase of the amplitude compared to the off-resonant cavity resonator’s amplitude ($H_{\text{ext}} \ll H_{\text{res}}$, cf. inset) below, at, and above the cavity’s resonance frequency.

Since the CMP can be regarded as the quasiparticle from a system of two coupled harmonic oscillators, the linewidth is found by fitting the sum of two Lorentzian functions to the

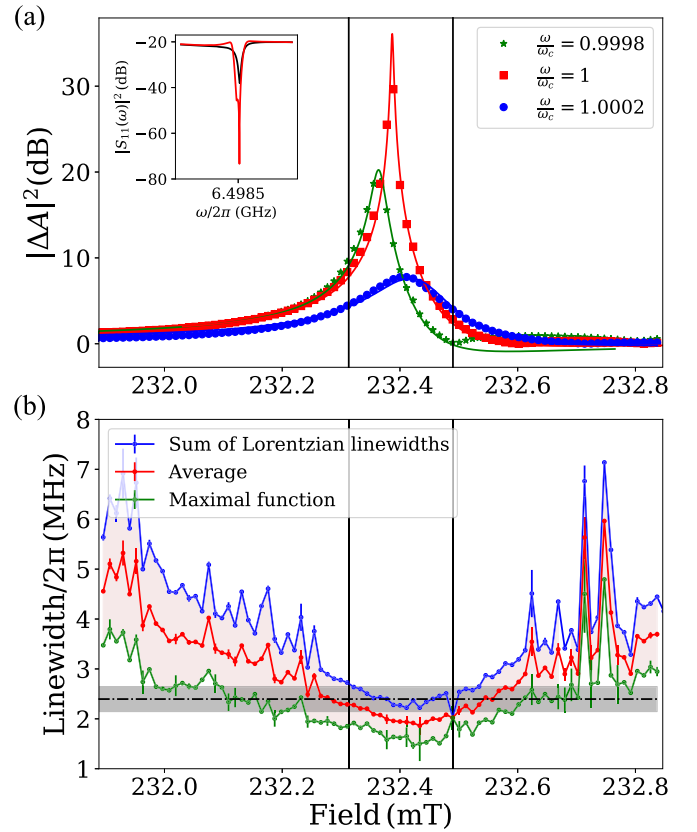


FIG. 4. (a) Absolute change $|\Delta A|^2$ in power units of the signal at level merging ($\delta_0 = 1.02 \pm 0.09$, $\phi = \pi$) corresponding to the absolute difference between the signal peaks off ($H_{\text{ext}} \neq H_{\text{res}}$, inset: black) and on ($H_{\text{ext}} = H_{\text{res}}$, inset: red) resonance below (green), at (red), and above (blue) $\omega_c/2\pi = 6.4985$ GHz. The inset shows the signal for ($\mu_0 H_{\text{res}} \approx 232.4$ mT), i.e., the maximal absolute change of 30 dB. The small kink is due to an asymmetry in the spectrum [cf. Fig. 2(b)II]. The absolute signal is increased for a field interval of $\approx \pm 0.1$ mT around resonance. The vertical lines show the area for a decreased linewidth at level merging and the solid lines are a fit to Eq. (1) at fixed frequency. (b) Field dependence of the linewidths between a lower bound (maximal function, green) and an upper bound (summed linewidth of two Lorentzians, blue) and the average (red). Around the field value for resonant coupling (vertical black bars), there is a decrease of the linewidth at level merging as the linewidth is lower than the geometric mean (dashed, including the error shown in gray) from the individual, off-resonant cavity photon and magnon linewidths. The invisible error bars of some data points are smaller than the marker size.

data and determined by the geometric mean between lower and upper bounds. While the lower bound is given by the maximal function, which always takes the higher value of the set of both linewidths [56], the upper bound is given by the sum of the individual linewidths. For a further decrease of the linewidth at level merging, the average from both bounds needs to be below the average of the off-resonant linewidths of magnon and cavity photon. They are determined to be $\kappa_r/2\pi = 3.79 \pm 0.003$ MHz and $\kappa_m/2\pi = 1 \pm 0.5$ MHz; i.e., the linewidth has to be below its geometric mean of 2.4 ± 0.25 MHz. On average, we observe an additional decrease of the linewidth by $\approx 13\%$ below the geometric mean including the error bar [gray shaded, cf. Fig. 4(b)]. This decrease in

level merging is supported by the observation of a corresponding increase in the total linewidth for $\phi = 0$ (cf. Fig. 4 in Ref. [49]).

IV. CONCLUSIONS

In summary, we demonstrated a method to achieve full control of the coupling strength of CMPs. This is done by tuning the relative phase ϕ and via the external attenuators the internal amplitude ratio δ_0 between the cavity photon's and magnon's AC magnetic fields (through a second port and the coupling into both ports). By controlling these parameters, we observe a full collapse of the anticrossing gap at resonance, a regime we call "level merging." This is observed only if the relative phase is set to $\phi = \pi$ as well as the relative amplitude ratio to $\delta_0 = 1$ [57]. We note that this transition, mediated by the two-toned system, is particularly interesting as it can be used to strongly increase the absolute amplitude of the signal. Moreover, our system realizes a fully automated tuning mechanism wherein we can easily shift through various levels of coupling, i.e., from level repulsion to recently studied level attraction [40]. We achieve level merging by externally controlling the coupling strength, whereas in other works, level attraction is observed by tuning the hybrid system's dissipation [25] or adding a "dielectric" contribution to the system [40,55]. With our system, it is also possible to deeply move into the regime of level attraction (using higher δ_0 's)

[58]. In our two-tone driven CMP experiment, however, the control over the coupling regime is realized without any direct changes of the experimental setup, thus reducing the error and being advantageous for real applications. Such an automated control mechanism over the spin-photon interaction could pave the way for deliberately turning the coherent exchange of information on and off. Furthermore, the presented spectroscopic two-tone control can be extended to time-dependent control to cavity-magnon polariton modes (cf. Ref. [59]). This could enable future applications for data storage and information processing by the addition of a nonlinear component such as a superconducting circuit to the spin-photon system.

ACKNOWLEDGMENTS

We acknowledge valuable discussions with Can-Ming Hu, Bimu Yao, Vahram L. Grigoryan, Ka Shen, and Ke Xia. This work is supported by the European Research Council (ERC) under the Grant Agreement No. 648011 and the DFG through SFB TRR 173/Spin + X. R. Macêdo acknowledges the support of the Leverhulme Trust. T. Wolz acknowledges financial support by the Helmholtz International Research School for Teratronics. R. Lebrun acknowledges the European Union's Horizon 2020 research and innovation programme under the Marie Skłodowska-Curie Grant Agreement FAST No. 752195.

-
- [1] D. L. Mills and E. Burstein, *Rep. Prog. Phys.* **37**, 817 (1974).
- [2] M. Litinskaya, in *Reference Module in Materials Science and Materials Engineering* (Elsevier, Amsterdam, 2016).
- [3] G. Kurizki, P. Bertet, Y. Kubo, K. Mølmer, D. Petrosyan, P. Rabl, and J. Schmiedmayer, *Proc. Natl. Acad. Sci. USA* **112**, 3866 (2015).
- [4] Y. Kubo, C. Grezes, A. Dewes, T. Umeda, J. Isoya, H. Sumiya, N. Morishita, H. Abe, S. Onoda, T. Ohshima, V. Jacques, A. Dréau, J.-F. Roch, I. Diniz, A. Auffeves, D. Vion, D. Esteve, and P. Bertet, *Phys. Rev. Lett.* **107**, 220501 (2011).
- [5] J. J. Morton and B. W. Lovett, *Annu. Rev. Condens. Matter Phys.* **2**, 189 (2011).
- [6] R. Blatt and D. Wineland, *Nature (London)* **453**, 1008 (2008).
- [7] R. Hanson and D. D. Awschalom, *Nature (London)* **453**, 1043 (2008).
- [8] I. M. Georgescu, S. Ashhab, and F. Nori, *Rev. Mod. Phys.* **86**, 153 (2014).
- [9] M. Aspelmeyer, T. J. Kippenberg, and F. Marquardt, *Rev. Mod. Phys.* **86**, 1391 (2014).
- [10] D. Angelakis, *Quantum Simulations with Photons and Polaritons: Merging Quantum Optics with Condensed Matter Physics*, Quantum Science and Technology (Springer, Berlin, 2017).
- [11] Y. Yamamoto, J. Jacobson, S. Pau, H. Cao, and G. Björk, in *Nanostructures and Quantum Effects* (Springer, Berlin, 1994), pp. 157–164.
- [12] J. M. Pitarke, V. M. Silkin, E. V. Chulkov, and P. M. Echenique, *Rep. Prog. Phys.* **70**, 1 (2006).
- [13] W. L. Barnes, A. Dereux, and T. W. Ebbesen, *Nature (London)* **424**, 824 (2003).
- [14] A. G. Gurevich and G. A. Melkov, *Magnetization Oscillations and Waves* (CRC Press, Boca Raton, FL, 2000).
- [15] I. Žutić, J. Fabian, and S. D. Sarma, *Rev. Mod. Phys.* **76**, 323 (2004).
- [16] Y. Tabuchi, S. Ishino, A. Noguchi, T. Ishikawa, R. Yamazaki, K. Usami, and Y. Nakamura, *Science* **349**, 405 (2015).
- [17] J. W. Lu, E. Chen, M. Kabir, M. R. Stan, and S. A. Wolf, *Int. Mater. Rev.* **61**, 456 (2016).
- [18] V. Baltz, A. Manchon, M. Tsoi, T. Moriyama, T. Ono, and Y. Tserkovnyak, *Rev. Mod. Phys.* **90**, 015005 (2018).
- [19] A. V. Chumak and H. Schultheiss, *J. Phys. D* **50**, 300201 (2017).
- [20] M. Harder and C.-M. Hu, in *Solid State Physics* (Elsevier, Amsterdam, 2018), pp. 47–121.
- [21] Ö. O. Soykal and M. E. Flatté, *Phys. Rev. Lett.* **104**, 077202 (2010).
- [22] Y. Tabuchi, S. Ishino, T. Ishikawa, R. Yamazaki, K. Usami, and Y. Nakamura, *Phys. Rev. Lett.* **113**, 083603 (2014).
- [23] D. F. Walls and G. F. Milburn, *Quantum Optics* (Springer-Verlag, Berlin, 2008).
- [24] Y. Choi, S. Kang, S. Lim, W. Kim, J.-R. Kim, J.-H. Lee, and K. An, *Phys. Rev. Lett.* **104**, 153601 (2010).
- [25] N. R. Bernier, L. D. Tóth, A. K. Feofanov, and T. J. Kippenberg, *Phys. Rev. A* **98**, 023841 (2018).
- [26] R. T. Juggins, J. Keeling, and M. H. Szymańska, *Nat. Commun.* **9**, 4062 (2018).
- [27] A. J. Moilanen, T. K. Hakala, and P. Törmä, *ACS Photon.* **5**, 54 (2018).
- [28] C. Dory, K. A. Fischer, K. Müller, K. G. Lagoudakis, T. Sarmiento, A. Rundquist, J. L. Zhang, Y. Kelaita, and J. Vučković, *Sci. Rep.* **6**, 25172 (2016).

- [29] L. Bai, M. Harder, Y. P. Chen, X. Fan, J. Q. Xiao, and C.-M. Hu, *Phys. Rev. Lett.* **114**, 227201 (2015).
- [30] X. Zhang, C.-L. Zou, L. Jiang, and H. X. Tang, *Phys. Rev. Lett.* **113**, 156401 (2014).
- [31] M. Harder, L. Bai, C. Match, and C.-M. Hu, *Sci. China Phys. Mech.* **59**, 117511 (2016).
- [32] M. Haidar, M. Ranjbar, M. Balinsky, R. K. Dumas, S. Khartsev, and J. Åkerman, *J. Appl. Phys.* **117**, 183906 (2015).
- [33] Y. Cao, P. Yan, H. Huebl, S. T. B. Goennenwein, and G. E. W. Bauer, *Phys. Rev. B* **91**, 094423 (2015).
- [34] B. Yao, Y. S. Gui, J. W. Rao, S. Kaur, X. S. Chen, W. Lu, Y. Xiao, H. Guo, K. P. Marzlin, and C. M. Hu, *Nat. Commun.* **8**, 1437 (2017).
- [35] X. Zhang, C.-L. Zou, N. Zhu, F. Marquardt, L. Jiang, and H. X. Tang, *Nat. Commun.* **6**, 8914 (2015).
- [36] D. Zhang, X.-Q. Luo, Y.-P. Wang, T.-F. Li, and J. Q. You, *Nat. Commun.* **8**, 1368 (2017).
- [37] Y. Yang, J. W. Rao, Y. S. Gui, B. M. Yao, W. Lu, and C.-M. Hu, *Phys. Rev. Appl.* **11**, 054023 (2019).
- [38] L. Liensberger, A. Kamra, H. M. Flaig, S. Geprägs, A. Erb, S. T. B. Goennenwein, R. Gross, W. Belzig, H. Huebl, and M. Weiler, *Phys. Rev. Lett.* **123**, 117204 (2019).
- [39] L. Bai, M. Harder, P. Hyde, Z. Zhang, C.-M. Hu, Y. P. Chen, and J. Q. Xiao, *Phys. Rev. Lett.* **118**, 217201 (2017).
- [40] M. Harder, Y. Yang, B. M. Yao, C. H. Yu, J. W. Rao, Y. S. Gui, R. L. Stamps, and C.-M. Hu, *Phys. Rev. Lett.* **121**, 137203 (2018).
- [41] V. L. Grigoryan, K. Shen, and K. Xia, *Phys. Rev. B* **98**, 024406 (2018).
- [42] B. Yao, T. Yu, Y. S. Gui, J. W. Rao, Y. T. Zhao, W. Lu, and C.-M. Hu, *Commun. Phys.* **2**, 161 (2019).
- [43] B. Bhoi, B. Kim, S. H. Jang, J. Kim, J. Yang, Y.-J. Cho, and S.-K. Kim, *Phys. Rev. Lett.* **99**, 134426 (2019).
- [44] Ferrisphere Inc., Flanders, NJ 07836, USA, <https://www.ferrisphere.com/>.
- [45] B. Zare Rameshti, Y. Cao, and G. E. W. Bauer, *Phys. Rev. B* **91**, 214430 (2015).
- [46] M. Goryachev, W. G. Farr, D. L. Creedon, Y. Fan, M. Kostylev, and M. E. Tobar, *Phys. Rev. Appl.* **2**, 054002 (2014).
- [47] I. Boventer, M. Pfirrmann, J. Krause, Y. Schön, M. Kläui, and M. Weides, *Phys. Rev. B* **97**, 184420 (2018).
- [48] M. Pfirrmann, I. Boventer, A. Schneider, T. Wolz, M. Kläui, A. V. Ustinov, and M. Weides, *Phys. Rev. Res.* **1**, 032023(R) (2019).
- [49] See Supplemental Material at <http://link.aps.org/supplemental/10.1103/PhysRevResearch.2.013154> for additional information on the determination of δ_0 , an estimate of the crosstalk, and the determination of the imaginary part of the coupling strength.
- [50] A. H. Morrish, *The Physical Principles of Magnetism* (John Wiley & Sons, New York, 2001), Chap. 10, pp. 539–639.
- [51] C. Kittel, *Phys. Rev.* **73**, 155 (1948).
- [52] P. Fletcher, I. H. Solt, and R. Bell, *Phys. Rev.* **114**, 739 (1959).
- [53] W. Yu, J. Wang, H. Y. Yuan, and J. Xiao, [arXiv:1907.06222v1](https://arxiv.org/abs/1907.06222v1).
- [54] B. Yao, T. Yu, X. Zhang, W. Lu, Y. Gui, C.-M. Hu, and Y. M. Blanter, [arXiv:1906.12142v1](https://arxiv.org/abs/1906.12142v1).
- [55] I. Proskurin, R. Macêdo, and R. L. Stamps, *New J. Phys.* **21**, 095003 (2019).
- [56] E. M. Stein and R. Shakarchi, *Real Analysis: Measure Theory, Integration and Hilbert Spaces* (Princeton University Press, Princeton, NJ, 2005).
- [57] C. Dörflinger, Master's thesis, Karlsruhe Institute of Technology (KIT), Karlsruhe, Germany, 2018.
- [58] I. Boventer, M. Kläui, R. Macêdo, and M. Weides, *New J. Phys.* **21**, 125001 (2019).
- [59] T. Wolz, A. Stehli, A. Schneider, I. Boventer, R. Macêdo, A. V. Ustinov, M. Kläui, and M. Weides, *Commun. Phys.* **3**, 3 (2020).